Experimental study on SFRC beams and slabs strengthened with FRCM composite materials

M.C. Rampini[1], G. Zani[2], M. Colombo[3] and M. di Prisco[4]

ABSTRACT: As shown in literature, Fabric-Reinforced Cementitious Matrix (FRCM) systems represent an effective solution to restore and upgrade the load carrying capacity of structural elements. In this paper, the flexural strengthening of Steel Fiber-Reinforced Concrete (SFRC) beams and slabs is investigated. The experimental campaign is focused on the mechanical characterization of the composite material, the evaluation of the interface bond-slip behavior and the verification of the FRCM reinforcement effectiveness by means of full-scale tests on beams and slabs. Structural elements are previously damaged at the ultimate limit state level and subsequently retrofitted. The results obtained and the comparison with theoretical predictions of the capacity increase are presented and discussed.

1 INTRODUCTION

In Italy, a newly introduced Italian standard allows the designers to use Fabric-Reinforced Cementitious Matrix (FRCM) composites to retrofit structural elements and to compute their capacity by combinations of tensile and shear bond tests (Consiglio Superiore dei LL. PP., 2018).
FRCM composites appear to be an effective solution in the retrofitting and strengthening interventions on damaged concrete structural elements (Anania, Badalà and D'Agata, 2016; Aljazaeri and Myers, 2018; Koutas *et al.*, 2018) and the advantages of this solution with respect to other techniques are the better compatibility with irregular surfaces and concrete substrate material, the easier workability and the smaller cost of installation (De Santis and De Felice, 2015). Their action depends on the tensile capacity and on the bond behavior with the substrate material. In this purpose, both direct tensile and shear tests were performed, considering different surface machining options (Rampini *et al.*, 2018).
To verify the effectiveness and to favor the widespread of the use of these composites in retrofitting interventions, the results of the full-scale test on retrofitted structural elements are presented and discussed. SFRC beams and slabs were previously damaged at the ultimate limit state and subsequently repaired by means of the application of an FRCM system, composed by a cementitious thixotropic mortar and an AR-glass fabric.
In the end, a preliminary tool to design the retrofitting interventions on pre-damaged elements is proposed, underlining the advantages and the critical issues.

2 MATERIAL CHARACTERIZATION

2.1 Steel Fiber-Reinforced Concrete (SFRC)

The material used to cast both beams and slabs is a self-compacting Steel Fiber-Reinforced Concrete (SFRC). An amount of 35 kg/m^3 of double hooked-end steel fibers (length 60 mm, diameter 0.9 mm, aspect ratio of about 65) was added to the mixture. Mix design and main properties are shown in di Prisco, Colombo and Pourzarabi, 2019. The identification of the multilinear tensile laws of SFRC is defined following the MC2010 provisions (CEB-FIP, 2010) at different ages (at 34 and 167/220 days). Stress-crack opening curves are depicted in Figure 1a, while, in Figure 1b, mode I stress-inelastic strain laws, implemented by using a characteristic length equal to the depth of the beam/slab sections (l_{cs}=150 mm), are shown. In the following, the stress-inelastic strain laws will be used in the plane-section analysis to predict the behavior of the structural elements in the pre-damaging phase.

[1] *PhD candidate, Politecnico di Milano, DICA Department, marcocarlo.rampini@polimi.it*
[2] *Postdoctoral fellow, Politecnico di Milano, DICA Department, giulio.zani@polimi.it*
[3] *Associate professor, Politecnico di Milano, DICA Department, matteo.colombo@polimi.it*
[4] *Full professor, Politecnico di Milano, DICA Department, marco.diprisco@polimi.it*

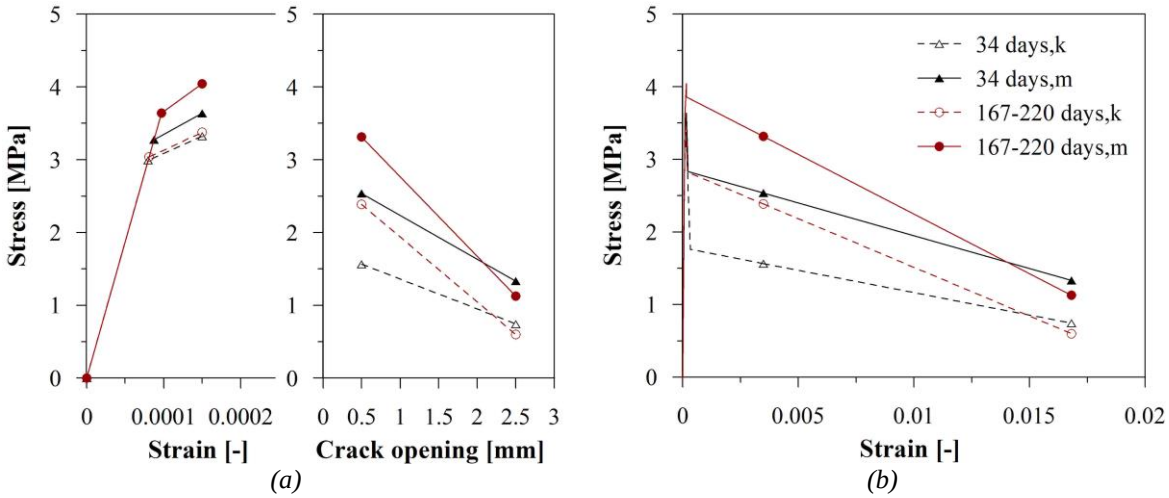

Figure 1. SFRC material constitutive laws: identification of multilinear tensile laws at different ages (a) and stress- strain laws obtained by using l_{cs}=150 mm (b).

2.2 Fabric-Reinforced Cementitious Matrix (FRCM) composite

The FRCM system that has been chosen to retrofit the structural pre-damaged elements is made by a shrinkage-compensated thixotropic cementitious mortar and an alkali-resistant glass double leno weave fabric, coated with an epoxy resin. The mortar is characterized by an average cubic compressive strength f_{cc} of 58.94 MPa, a flexural tensile strength f_{ctf} equal to 7.02 MPa, and an elastic modulus E_c of 28 GPa, as declared by the manufacturer. The main properties of the fabric are summarized in Table 1. The maximum average tensile load is evaluated on five uniaxial tests for each direction, following the procedure described in ISO 4606 (International Organization for Standardization, 1995). The efficiency parameter EF_f of the glass textile in tension, evaluated as proposed by Rampini *et al.*, 2019, represents important information on the rate of utilization of the reinforcement materials.

Table 1. Alkali-resistant glass fabric characteristics.

Characteristic	warp	weft
Wire spacing [*mm*]	*38*	*38*
Roving fineness [*Tex*]	*2 x 2400*	*4 x 2400*
Filament diameter [μm]	*27*	*27*
Eq. thickness [*mm*]	*0.093*	*0.093*
$P_{max,avg}$ [*kN*]	*12.50**	*11.70*
Fabric efficiency EF_f	*0.87*	*0.82*

**average on four samples*

The curves in Figure 2 represent the uniaxial tensile behavior of three nominally identical FRCM specimens (70 × 400 × 9 mm^3 in size) tested imposing a constant stroke rate of 0.02 mm/s. The responses are depicted in terms of nominal stress on the FRCM cross section vs. normalized displacement (stroke/free length), computed over a free length of around 300 mm. Please note (Figure 2) that, when one of the load-stroke curves is lost, the average response is still evaluated considering the remaining specimens, then the peaks represent the best performing sample. The efficiency parameters EF_{FRCM}, on the contrary, are evaluated dividing the mean maximum load, 9.13 kN in the warp and 7.00 kN in the weft directions, by the one on the plain fabric, resulting in values equal to 0.73 and 0.60, respectively. The maximum load reached during the test is strongly influenced by the anchorage length and the misalignment between the fabric wires and the tensile direction. A greater value of efficiency can be generally achieved testing composites with a larger anchorage and a specimen wide enough to have more than two

wires within the section, allowing stress re-distribution, hence reducing the possibility to obtain a lower load capacity due to misalignment.

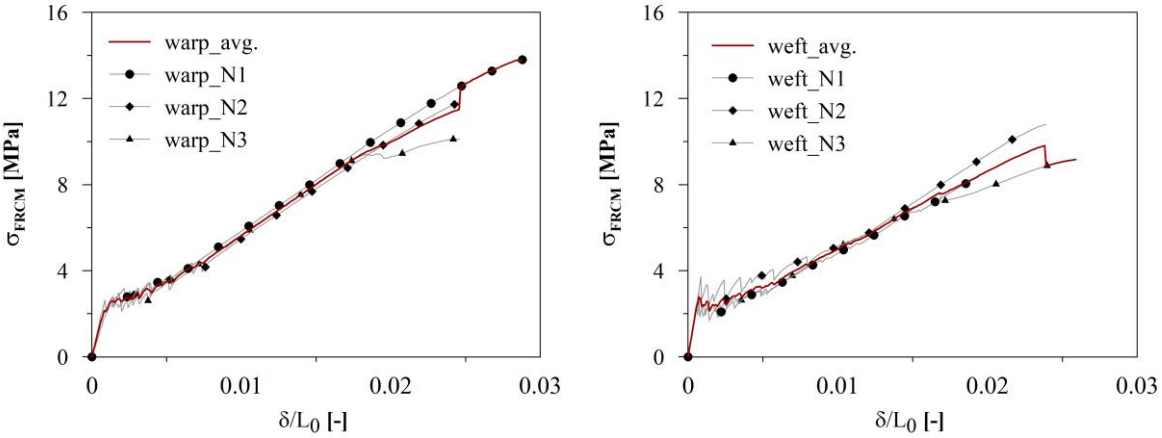

Figure 2. Average tensile responses of the FRCM system in terms of nominal stress vs. normalized displacement in the warp (a) and weft directions (b).

3 SHEAR SINGLE LAP TESTS

In order to characterize the bond-slip behavior at the interface level between the FRCM composite and the substrate, shear bond tests were carried out using a single-lap (SL) setup, Figure 3a. Test specimens ($70 \times 200 \times 9$ mm^3 in nominal size) were manufactured applying a FRCM reinforcement strip on a concrete substrate, considering two different machining options: sand-blasting, (s), for two specimens and hydro-scarification, (h), with a pressure of 1800 atm, for three supports. The application was done casting the composite by means of a typical hand lay-up technique and following recommendations provided by the mortar suppliers in order to guarantee adequate adhesion of the reinforcement to the surfaces. An epoxy resin tab was preliminary created at the end of the unbonded fabrics to prevent slippage phenomena and failure of the textile due to stress localization within the clamping zone. Please note that all the fabrics are placed with the warp direction parallel to the applied load.

The tests were performed under displacement control at a 0.01 mm/s stroke rate. In addition to the stroke output, 2 Linear Variable Differential Transformer (LVDT) transducers were placed, so as to measure the relative displacement ($\delta_{slip,sx/dx}$) among the support and the head of the reinforcement layer.

In Figure 4 the responses of the different specimens in terms of load-stroke and load-slip are set out and it is possible to appreciate the different bond-slip behavior considering different surface roughness. Please note that the results are averaged according to the same procedure of the tensile tests. In both the SL(s) specimens the failure was due to the delamination of the reinforcement from the support and the average value of shear stress is equal to 0.39 MPa (Figure 3b). It can be noticed that the slippage is instantaneously activated at the occurrence of failure (Figure 4a). Regarding the hydro-scarificated specimens, the collapse occurred in three different ways, Figures 3c-e and 4b: i) fabric rupture for the SL(h)$_1$ case, where the slip value remains constantly close to zero up to the end of the test; ii) tensile failure of the textile within the matrix with subsequent partial ejection of the external layer of mortar for the SL(h)$_2$ specimen; and iii) global ejection of the external layer of mortar alongside a partial sliding of the textile for the SL(h)$_3$ one. In Table 2, the maximum load values are summarized, together with the description of the failure modes according to RILEM recommendations (de Felice *et al.*, 2018).

As expected, the greater roughness observed in the hydro-scarificated specimens improves the mechanical adhesion at the interface, increasing both the global capacity and the effectiveness of the FRCM reinforcement.

The maximum load reached in the case of the hydro-scarificated substrates resulted greater than the average direct tensile load of the plain FRCM in the warp direction. This means that in the

design of the retrofitting application, according to the Italian guidelines, the full tensile capacity of the composite material can be considered.

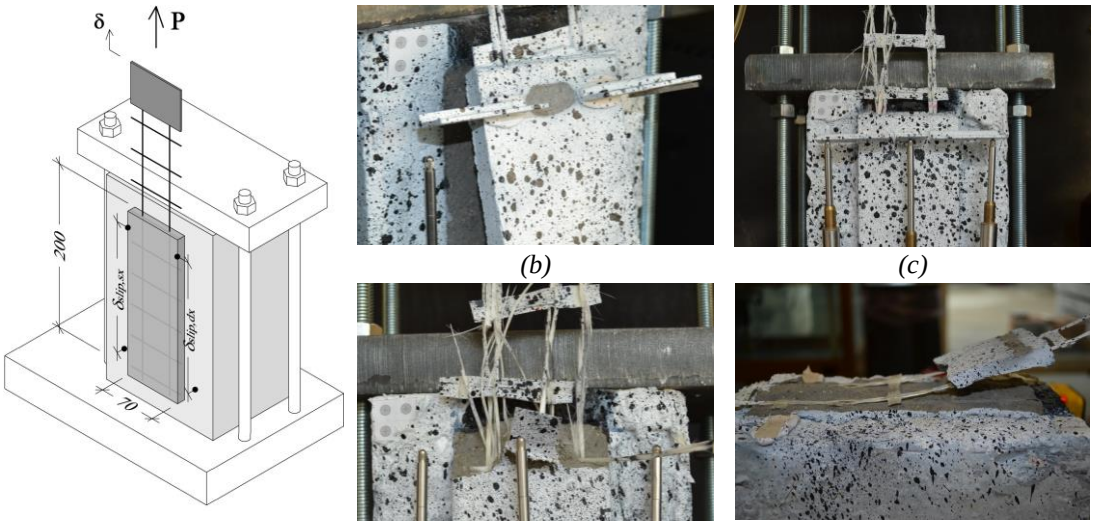

Figure 3. Single lap shear test setup (a) and example of different failure modes: SL(s)$_{1-2}$ (b), SL(h)$_1$ (c), SL(h)$_2$ (d) and SL(h)$_3$ specimen (d).

Table 2. Single lap shear test results: maximum loads and failure modes identification following RILEM recommendations (de Felice *et al.*, 2018).

Specimen	P_{max} [kN]	Failure modes
SL(s)1	*4.44*	*Detachment at matrix-to-substrate interface*
SL(s)2	*6.42*	*Detachment at matrix-to-substrate interface*
SL(h)1	*9.29*	*Tensile failure of the textile out of the matrix*
SL(h)2	*9.88*	*Tensile failure of textile within the matrix + external matrix layer (partial) ejection**
SL(h)3	*10.02*	*(Partial) Sliding of the textile within the matrix + external matrix layer global ejection**

**different from the RILEM failure modes descriptions*

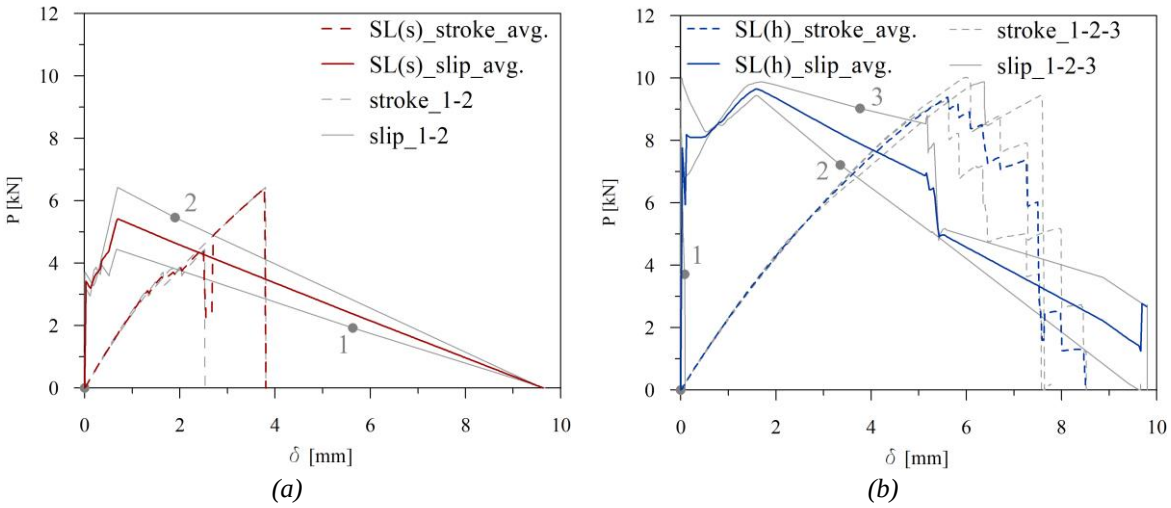

Figure 4. Single lap shear test responses: Load-stroke and Load-slip curves for SL(s), sandblasted (a) and SL(h), hydro-scarificated supports (b).

4 FULL-SCALE TESTS ON FRCM REINFORCED BEAMS AND SLABS

4.1 Reinforced SFRC beams test responses

Two SFRC beams (350 × 1450 × 150 mm^3) were preliminary damaged in four-point bending considering a span equal to 1350 mm and a distance between the loading knives of 450 mm. The test was displacement controlled imposing a constant stroke rate of 3 μm/s. To measure the crack opening displacements (COD) on the intrados and the axial compression displacement, six (3+3) LVDT transducers were applied to the specimen bottom/top surfaces, while, to measure the mid-span deflection, two Potentiometer Displacement Transducers (PDT) were used. The gauge lengths are 300 mm and 500 mm, respectively for COD and COM measurements. The pre-damage tests were performed after more than 200 days from the casting date.
After the pre-damage phase, the two beams were reinforced with a one-layer AR-glass fabric FRCM system, as the one described in the material characterization section. Fabric was oriented with the warp parallel to the longitudinal direction of the beam. The reinforcement layer was 20 mm thick, 350 mm wide (9 warp wires) and was applied to the bottom surface of the beam, on a total length of 1.2 m. In order to prevent delamination failures, the substrate bottom surfaces were hydro-scarificated by using the same water pressure (around 1800 atm) of the shear single-lap specimens. The two reinforced beams were tested with the same setup of the pre-damage test, Figure 5a, applying an identical displacement rate.

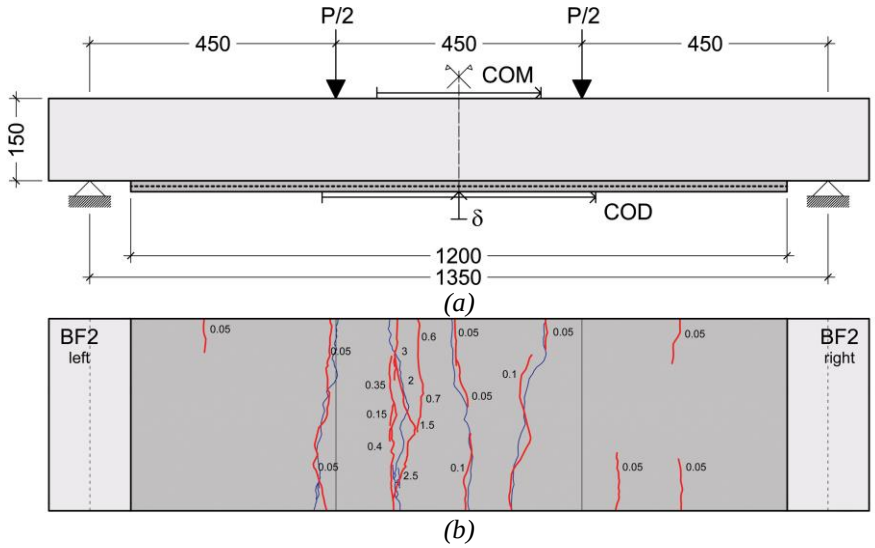

Figure 5. Four-point bending test scheme and instruments arrangement (a). Cracking pattern (b) on the intrados after the pre-damaged test (blue) and the post-reinforced test (red). Crack openings refer to the post-reinforced beams. [Dimensions are in mm].

The comparison between the pre-damage responses and the post-reinforcement ones is shown in Figure 6. The result of the rehabilitation procedure is the recovery of the full capacity of the members in terms of both ultimate load and deformation. The average ultimate load reached is equal to 39.69 kN, with an increase of about 28% with respect to the previous maximum one ($P_{max,pre,avg}$=31.05 kN), corresponding to around three times the residual capacity ($P_{res,pre,avg}$=11.53 kN) before the application of the FRCM reinforcement.
Looking at the first part of the pre/post curves in Figure 6-7, it is also possible to notice that the addition of a 20 mm-thick layer of FRCM allows to fully recover the initial stiffness, up to the cracking of the mortar layer.
The crack pattern of the post-reinforced beam at the end of the test is compared with the one present before the surface machining (Figure 5b). It is important to underline that the number of visible cracks in the measuring zone present after the pre-damaging phase is equal to 1 and 3, for the BF1 and BF2 respectively. The post-reinforced cracking pattern is strongly influenced by the previous damage; in fact, the FRCM system moderately increases the number of visible cracks, opening a few of them near the already present ones.

The added FRCM layer could stabilize the cracking mechanism of the SFRC, better exploiting the residual capacity of the internal SFRC material. As a matter of fact, the different behavior between the two beams in the pre-damage tests (probably connected to uneven distribution and orientation of steel fibers) is reflected in different post-reinforcement responses in terms of maximum load and global crack opening displacement (Figure 6-7). Moreover, after the tensile rupture of the AR-glass fabric, that corresponds to the peak in the load-deflection curve, it is possible to observe a reduction of the sustained load controlled by the residual capacity of the SFRC.

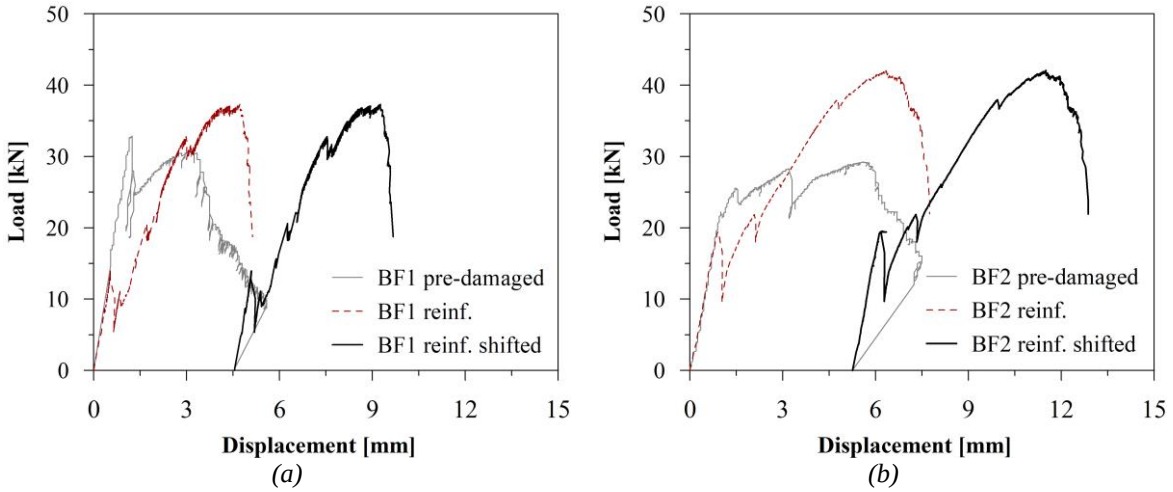

Figure 6. Load vs. mid-span displacement responses of pre-damaged SFRC beams strengthened with FRCM composite material: slab BF1 (a) and BF2 (b).

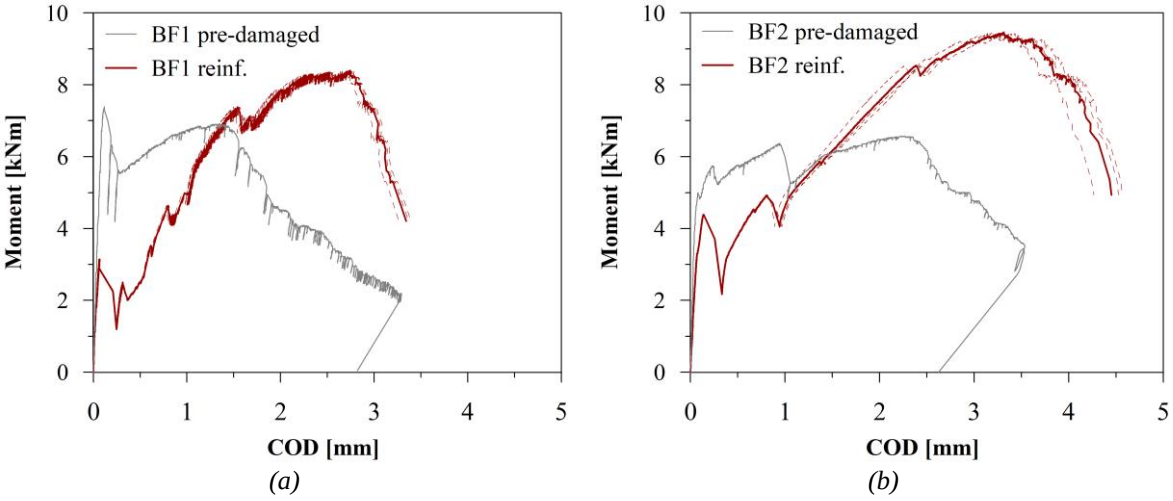

Figure 7. Moment vs. COD curves of pre-damaged FRC beams strengthened with FRCM composite material: beam BF1 (a) and BF2 (b).

4.2 Reinforced SFRC slabs test responses

The procedure of pre-damaging, reinforcing and testing the two SFRC slabs is analogous to the one described for the SFRC beams. The setup configuration of the full-scale tests is depicted in Figure 8a, together with the nominal dimensions of the two slabs and the instruments configuration. Both the pre-damage and the post-reinforced tests were displacement controlled at a stroke rate equal to 20 and 25 μm/s, respectively. The initial gauge lengths of the COD measurements are 300 mm for the superior/inferior ones and 1000 mm for the longer ones on the bottom side of the slabs. The loading and the supports areas have a square shape with a 200 mm side. Also in this case, the tests were performed more than 200 days after the SFRC casting.

Following the hydro-scarification, the FRCM reinforcement was applied on the bottom surface of the two slabs arranging two 1 m wide strips of AR-glass fabric (26 warp wires) in the cross-way directions. This choice was done in order to have a symmetric disposition of the FRCM system, crossing two fictitious reinforced beams spanning between opposite supports.

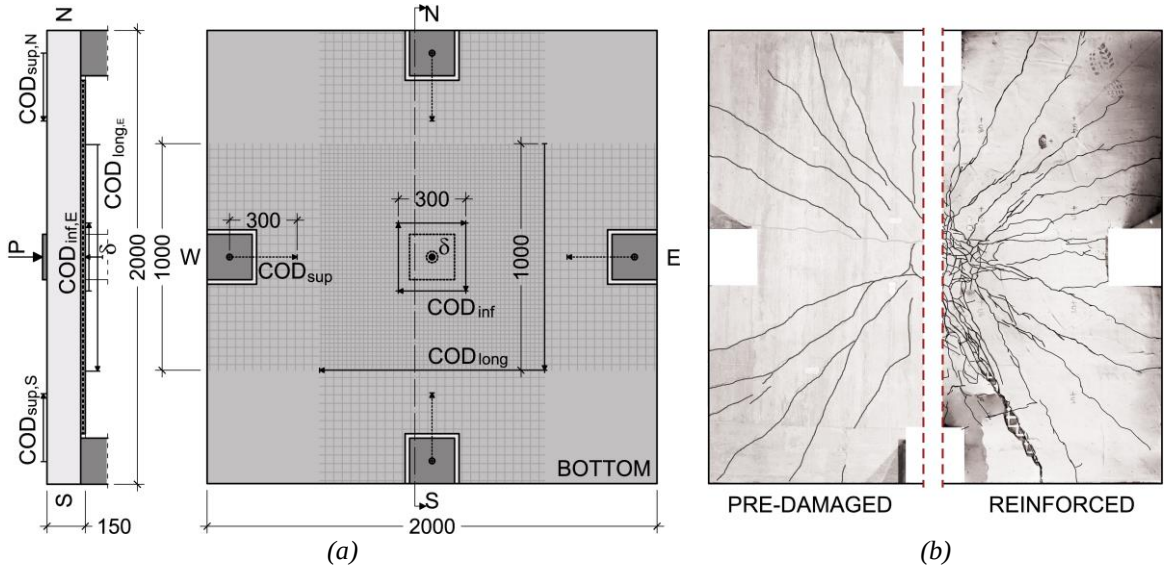

(a) *(b)*

Figure 8. Slab tests scheme and instruments disposition (a). Crack pattern at the intrados surface of the SF2 slab (b). [Dimensions are in mm].

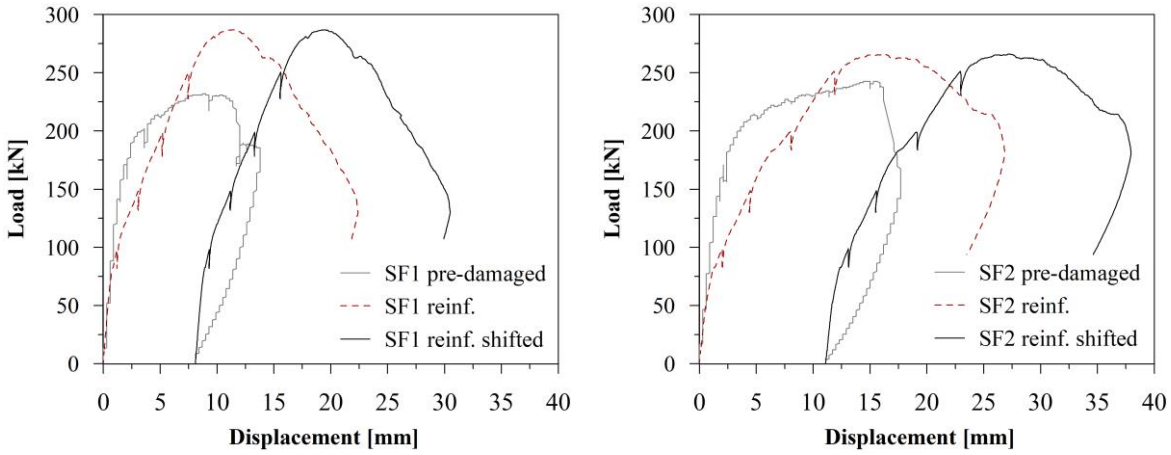

(a) *(b)*

Figure 9. Load vs. displacement responses of pre-damaged SFRC slabs strengthened with one layer of FRCM composite material: slabs SF1 (a) and SF2 (b).

In Figure 9, the load-displacement curves of both pre-damage and post-reinforcement tests are represented. The average maximum load reached in the post-reinforced tests is equal to 276.64 kN, corresponding to an increase of 17% and 58% with respect to the mean maximum and the residual loads of the pre-damage tests (237.29 kN and 175.03 kN).

As in the beams, the initial stiffness seems to be almost completely recovered and, regarding the softening behavior after the peak, the FRCM layer acts to maintain the residual capacity of the internal material and to prevent a rapid decrease of the load, thanks to the 2D disposition of the textile. The rupture of the textile is also associated with the partial ejection of the external mortar layer.

At the response peaks, the crack opening read from the instruments in the two tests are comparable, as shown in Figure 10, while the total number of cracks created in the post-reinforcement

case is larger (Figure 8b). This means that the FRCM composite is able to control the crack openings, also if the substrate material is strongly damaged.
Regarding the extrados crack opening, the measurements in both tests remain close to zero. This means that there are no cracks opened on the top surface and the supports can be assumed as hinges; this assumption will be considered in the following prediction analysis.

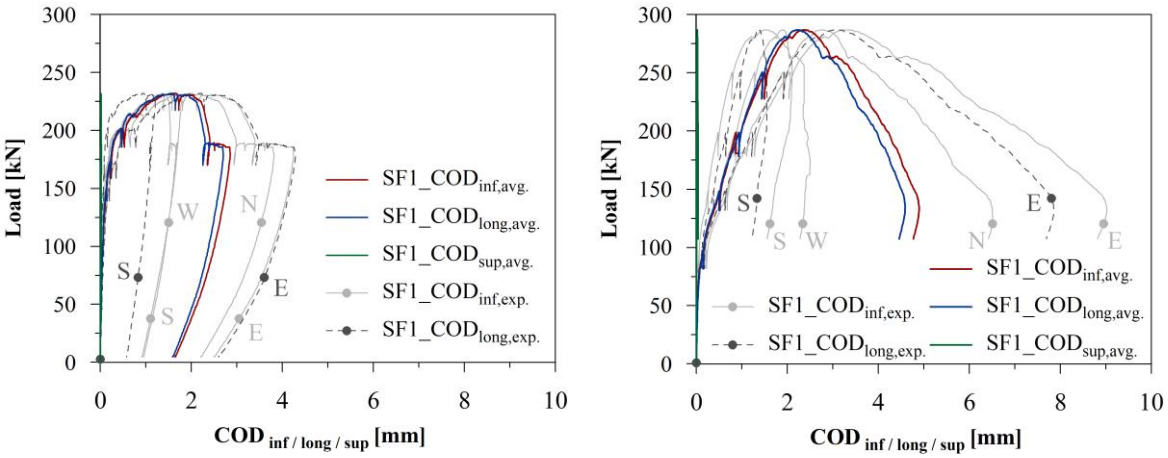

Figure 10. Load vs. COD curves of SFRC slabs in the pre-damaged test (a) and in the post-reinforced test (b).

5 SIMPLIFIED APPROACH TO PREDICT THE STRUCTURAL CAPACITY OF REINFORCED BEAMS AND SLABS

In order to obtain a prevision of the maximum capacity of the FRCM reinforced beams and slabs, the simplified procedure described step by step in the following was performed. This analysis is aimed at evaluating the amount of the sustained load due to the additional FRCM layer applied to the intrados of the elements, to be added to the residual capacity of the pre-damaged members.
The first step was to evaluate the response for both pre-damaged beams and slabs, using the different multilinear constitutive laws for the SFRC material, Figure 1b. In the case of SFRC beams, the experimental moment-COD curves are directly compared with the analytical ones obtained by using a plane-section approach, Figure 11a. The analytical COD, as it was done for the multilinear constitutive laws, is computed considering a characteristic length equal to the depth of the section, 150 mm. The choice to have only one value of this length for the two beams, independent from the experimental crack pattern observed at the end of the test, was selected in order to have a provisional estimation of the responses. Moreover, observing the cracking pattern obtained from the pre-damaging tests the chosen value is close to the mean distance between cracks, 125 mm for the BF2 beam.
The same sectional approach was also used in the analysis of the slabs pre-damaging responses. In this case, the comparison was done computing the maximum load capacity by using the well-known strip method (Hillerborg, 1975), considering the slab as a couple of two simply supported fictitious beams that work in parallel in three-point bending. The span length is taken equal to 1.8 m (the total width of the slab minus two times half of the support side) while the value of the width is variated among the analyses. The results are summarized in Figure 11b, where it is possible to see the variation of the estimated maximum load due to the choice of different SFRC constitutive laws and fictitious beam widths.
The second step of the analysis was to assume that the increment of the bending moment capacity of a section, due to the addition of the FRCM layer, could be computed multiplying the ultimate tensile force of the composite (referred to the actual number of wires) by the internal level arm of a fictitious section where the pre-damaged SFRC is considered elastic in compression and with zero strength in tension. For each member, the internal level arm is calculated

from the neutral axis position at the peak response of the best-fitting analytical simulation (characteristic tensile law at 167-220 days for beams and average tensile law at 167-220days with a fictitious beam width of 1.5 m for slabs).

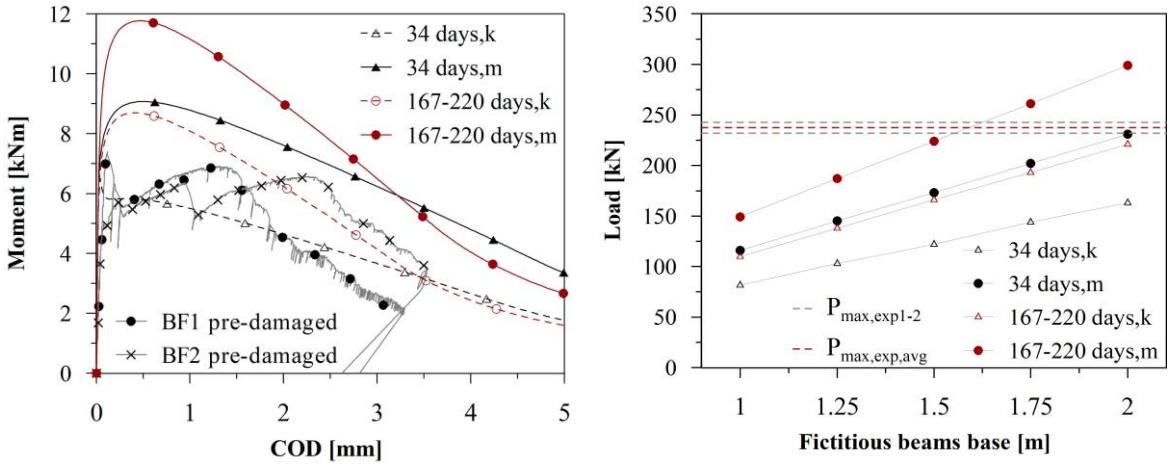

(a) *(b)*

Figure 11. Prediction of the pre-damaged moment vs. COD response for SFRC beams (a) and of the maximum load capacity of SFRC slabs (b).

In the end, the additional bending moment capacity evaluated before is used to compute the load increment by imposing the equilibrium on the above-mentioned structural schemes (four-point bending for BF1-2 and two fictitious beams for SF1-2).
The results of the simplified procedure are shown in Figure 12 and the average estimated peaks are 38.92 kN for reinforced beams and 254.15 kN for slabs, respectively corresponding to 98% and 92% of the experimental values.

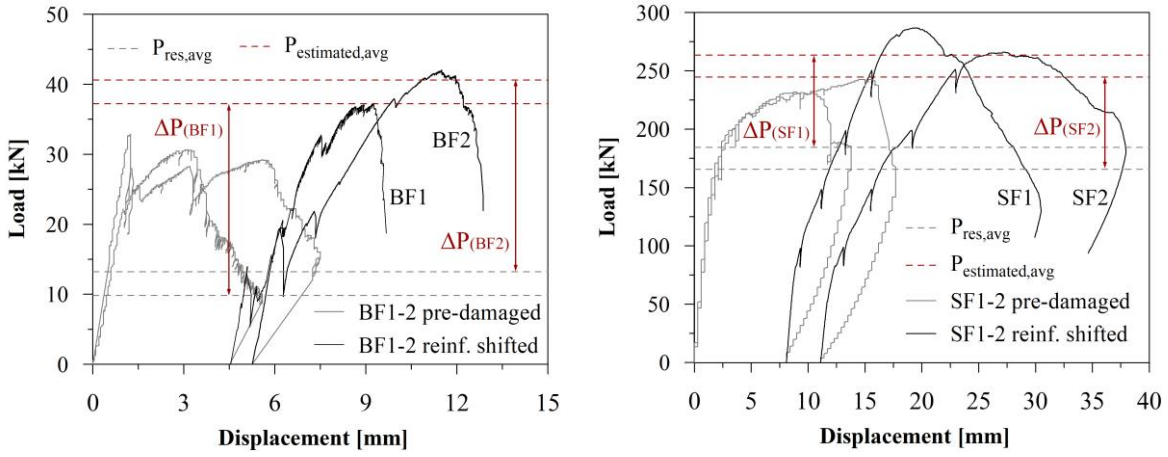

(a) *(b)*

Figure 12. Analytical estimation of the maximum capacity after the application of the FRCM reinforcement for SFRC beams (a) and slabs (b).

6 CONCLUSIONS

Based on the results presented in this paper, it is possible to draw some conclusions: 1) the estimation of the responses in the pre-damaging phase confirms that, given different constitutive laws of SFRC characterized at different material ages, the structural response of beams settles to the characteristic one while, due to the stresses redistribution capacity, the behavior of the slab approaches the average one; 2) a correct substrate machining guarantees the efficiency of the reinforced capacity of the FRCM layer, preventing weak/brittle failure mechanism in the

global response (i.e. delamination); 3) the FRCM reinforcement technique seems to be adequate to restore both the peak capacity under flexural actions and the stiffness of the integer substrate specimens; 4) the FRCM layers act stabilizing the residual behavior of the internal SFRC and increasing the global energy dissipation; 5) the simplified analysis presented at the end of the paper represents an effective tool for the preliminary design of retrofitting interventions on pre-damaged structural members.

7 ACKNOWLEDGEMENTS

The authors would like to acknowledge Gavazzi Tessuti Spa and BASF Italia Spa for their precious contribution to the research. The research was financially supported by RELUIS WP14 – 2019/2021.

8 REFERENCES

Aljazaeri, Z. R. and Myers, J. J. (2018) 'Flexure Performance of RC One-Way Slabs Strengthened with Composite Materials'. doi: 10.1061/(ASCE)MT.1943-5533.0002299.

Anania, L., Badalà, A. and D'Agata, G. (2016) 'Numerical simulation of tests for the evaluation of the performance of the reinforced concrete slabs strengthening by FRCM', *Curved and Layered Structures*, 3(1), pp. 63–73. doi: 10.1515/cls-2016-0005.

CEB-FIP (2010) *Model Code 2010 - Volume 1, fib Model Code for Concrete Structures 2010*. doi: 10.1002/9783433604090.ch6.

Consiglio Superiore dei LL. PP. (2018) 'Linea Guida per la identificazione, la qualificazione ed il controllo di accettazione di compositi fibrorinforzati a matrice inorganica (FRCM) da utilizzarsi per il consolidamento strutturale di costruzioni esistenti', pp. 1–5. doi: 10.1109/ChiCC.2015.7260208.

de Felice, G. *et al.* (2018) 'Recommendation of RILEM Technical Committee 250-CSM: Test method for Textile Reinforced Mortar to substrate bond characterization', *Materials and Structures/Materiaux et Constructions*, 51(4), pp. 1–9. doi: 10.1617/s11527-018-1216-x.

Hillerborg, A. (1975) *Strip method of design*. Cement and Concrete Association. Available at: https://trid.trb.org/view/49789 (Accessed: 23 May 2019).

International Organization for Standardization (1995) 'ISO 4606:1995 Textile glass -- Woven fabric -- Determination of tensile breaking force and elongation at break by the strip method', pp. 1–16. Available at: https://www.iso.org/standard/10541.html (Accessed: 23 May 2019).

Koutas, L. N. *et al.* (2018) 'Strengthening of Concrete Structures with Textile Reinforced Mortars: State-of-the-Art Review', *Journal of Composites for Construction*, 23(1), p. 03118001. doi: 10.1061/(asce)cc.1943-5614.0000882.

di Prisco, M., Colombo, M. and Pourzarabi, A. (2019) 'Biaxial bending of SFRC slabs: Is conventional reinforcement necessary?', *Materials and Structures/Materiaux et Constructions*. Springer Netherlands, 52(1), pp. 1–15. doi: 10.1617/s11527-018-1302-0.

Rampini, M. C. *et al.* (2018) 'Textile reinforced concrete composites for existing structures: Performance optimization via mechanical characterization', in *Proceedings of the 12th fib International PhD Symposium in Civil Engineering*.

Rampini, M. C. *et al.* (2019) 'Mechanical Behaviour of TRC Composites: Experimental and Analytical Approaches', *Applied Sciences*, 9(7), p. 1492. doi: 10.3390/app9071492.

De Santis, S. and De Felice, G. (2015) 'Tensile behaviour of mortar-based composites for externally bonded reinforcement systems', *Composites Part B: Engineering*. Elsevier Ltd, 68, pp. 401–413. doi: 10.1016/j.compositesb.2014.09.011.